Supplemental Methods:

Mouse erythroblast collection and fluorescence staining.

Mouse fetal livers were dissected in PBS ($Ca^{++}Mg^{++}$-free, Gibco 14190-136), mechanically dissociated and fixed overnight in 4% PFA in PBS at 4°C. Cells were washed in PBS several times, centrifuged in an Eppendorf microfuge at 4000 rpm for 4 minutes, re-suspended in permeabilization buffer (0.3% Triton X-100 in PBS), and incubated for 10 minutes at room temperature. Cells were stored in blocking buffer (3% BSA/1% goat serum in PBS) at least overnight at 4°C. Spleen cells were mechanically dissociated and fixed, washed and blocked as described for fetal liver cells. To collect bone marrow cells, both femurs from a mouse were cleaned of tissues and rinsed in PBS. The top and bottom were cut off the femur and the bone marrow was flushed out with a 27-gauge syringe filled with PBS into 12-well plate. Cells were mechanically dissociated, fixed in 4% PFA in PBS overnight, permeabilized as above and stored in blocking buffer at least overnight at 4°C. In some experiments, erythroblasts were fixed for 30 minutes or 4 hours at RT in 4% PFA in PBS; results were similar to overnight fixation (data not shown).

Blocked cells were stained in solution for 2 hours at RT or overnight at 4°C with primary antibodies (Supplemental Table 2) diluted in blocking buffer. After washing, cells were stained for 2 hours at RT with secondary antibodies (Supplemental Table 3) diluted in blocking buffer including either rhodamine-phalloidin (1:100, Invitrogen, Grand Island, NY) or Alexa 647-phalloidin (1:100, Invitrogen) to stain F-actin, and Hoechst 33258 (1:1000, Invitrogen) to stain nuclei. Cells were then deposited onto slides using a Thermo Scientific Cytospin 4 cytocentrifuge at 1000 rpm for 3 minutes, coverslipped with Fluoro-Gel (Electron Microscopy Sciences, Hatfield, PA), and imaged within seven days.

Human bone marrow erythroblast collection and fluorescence staining:

Human bone marrow erythroblasts were obtained from normal human donors providing bone marrow transplant samples. Cells were obtained from the discarded bag used for bone marrow collection within 2-4 hours, and mature red blood cells were lysed using ammonium chloride (EasySep Red Blood Cell Lysis Buffer, Stem cell Technology, Vancouver, Canada) for 15 minutes at RT. After centrifugation (300 g, 10 minutes, RT), the cell pellet was fixed in 4% PFA in PBS overnight on ice. Samples were washed in PBS several times and permeabilized in 0.3% Triton X-100 in PBS for 10 minutes at room temperature. Cells were resuspended in blocking buffer (3%BSA/1% goat serum in PBS) and stored at least overnight at 4°C, and then immunostained as described above for mouse erythroblasts. To locate the GPA-positive polarized or enucleating erythroblasts amongst the numerous earlier stage erythroblasts, non-erythroid cells and mature red blood cells in the human bone marrow aspirate samples, the entire slide was scanned in the confocal microscope, and Z stacks were acquired for each field containing a polarized or enucleating erythroblast. Z stack acquisition parameters are described in the Methods.

Fluorescence image quantitation:

Measurements of cell surface constriction diameter at the Ter119 (mouse) or GPA (human) sorting boundary, nucleus diameter at the Ter119/GPA sorting boundary, extent of nuclear protrusion past the sorting boundary, and total nuclear length along the long axis, were done on extended focus (maximum intensity) projections of stacks of enucleating cells using Volocity 6.3 (Perkin Elmer). 3D visualization of F-actin in erythroblasts was performed using the 3D opacity function in Volocity 6.3, and F-actin spot volume measurements were done with the Volocity measurement module using the ‘find object’ tool.

Transmission Electron Microscopy:

E14.5 fetal mouse livers were removed and fixed overnight in ice-cold 4% paraformaldehyde and 1.5% glutaraldehyde in 0.1 M Na-cacodylate buffer. The following day, the tissues were cut into small pieces and the fixative was exchanged with 2.5% glutaraldehyde in 0.1 M Na-cacodylate buffer for an additional overnight incubation. Subsequent treatments consisted of a buffer wash, postfixation in buffered 1% osmium tetroxide for 2 hours, washed in distilled water and then dehydrated in graded ethanols followed by propylene oxide. Tissue pieces were embedded in Embed 812 / Araldite (Electron Microscopy Sciences, Hatfield PA). After polymerization, semi thick sections (1 µm) were cut, mounted on glass slides and stained in toluidine blue for general assessment in the light microscope. Subsequently, 60 nm thin sections were cut with a diamond knife (Diatome, Hatfield PA), mounted on copper slot grids coated with parlodion and stained with uranyl acetate and lead citrate for examination on a Philips CM100 electron microscope (FEI, Hillsbrough OR). Images were documented using a Megaview III CCD camera (Olympus Soft Imaging Solutions GmbH, Münster, Germany). Images were subsequently handled in Adobe Photoshop.

Flow cytometry of mouse fetal liver cells.

Fetal liver cells (wild type or *Tmod1*$^{-/-}$) were resuspended in PBS containing 0.5% (weight/volume) BSA and 2mM EDTA, and erythropoiesis was monitored by flow cytometry as previously described[1,2]. After removing leukocytes by magnetic selection (CD45 microbeads, 10µl/10^7 cells 15 minutes on ice; Miltenyi Biotech), cells were then washed once in PBS 0.5% BSA 2mM EDTA and magnetic separation was performed using MACS LS columns (Miltenyi Biotech) according to manufacturer instructions. Cells (10^6/80µl) were resuspended in PBS with 0.5% BSA and blocked with a rat anti-mouse CD16/CD32 antibody (2.5 µg/10^6 cells) for 15 minutes on ice. Cells were then stained using a cocktail of CD45R/Ly6G/CD11b-APC-Cy7-conjugated (0.3µg/10^6 cells each), Ter119-FITC (1µg/10^6 cells each) and CD44-APC-

conjugated (0.5μg/ml) for 15 minutes at RT[2]. In separate tubes, cells were stained with Hoeschst33342 and Ter119-FITC (1μg/10^6 cells each) to measure the percentage of enucleation. Fluorescence was evaluated using a BD Fortessa (Beckton Dickinson) flow cytometer and data were subsequently analyzed using FlowJo v10.3 (Tree Star Inc.).

CD34+ cell isolation and erythroid culture:

CD34+ cells from cord blood were isolated by positive selection, using the Magnetic Activated Cell Sorting (MACS) beads system (Miltenyi Biotec, San Diego, CA), according to the manufacturer's instructions. CD34+ cells were then induced to erythroid differentiation using a 3-phase liquid culture system over a period of 18 days as described previously[3]. Differentiation was assessed by flow cytometry, using Glycophorin A (GPA), Band 3 and α4-integrin as surface markers. Representative flow cytograms for Day 11 and Day 15 of differentiation are presented in Supplemental Figure 8. Fluorescence was evaluated using a BD Fortessa (Becton Dickinson) flow cytometer and data were subsequently analyzed using FlowJo v10.3 (Tree Star Inc.).

Fluorescence-activated cell sorting of cultured human erythroid cells and enucleation assay:

To assess enucleation in control or *TMOD1* knocked down cells, cells at D16 of culture were sorted following staining procedures provided in Hu et al.[3] using the BD FACSAria™ sorter. Orthochromatic erythroblasts were sorted based on GPA and Band3 positive expression and low expression of α4-integrin. Live cells were collected by exclusion of DAPI positive populations. These orthochromatic erythroblasts were put back into culture (Phase III of the culture system) for one hour, at 37ºC, 5%CO_2. The percentage of enucleation was determined by flow cytometry of sorted orthochromatic erythroblasts, using the fluorescent probe SYTO60 (Life Technologies) as described previously[4]. Fluorescence was evaluated using a BD Fortessa (Becton Dickinson) flow cytometer and data were subsequently analyzed using FlowJo v10.3

(Tree Star Inc.).

Erythroblast morphology from CD34+ erythroid cultures

Samples of 10^5 cells were collected at Days 7, 11, 15 post *in-vitro* culture, or after cell sorting of cultures for orthochromatic erythroblasts, and cytocentrifuged onto a glass microscope slide at 300 rpm for 10 minutes. Cytospins were stained with May-Grunwald Giemsa, and images were acquired with a 60X oil immersion objective (EVOS® FL Auto Imaging System).

Lentivirus, transduction, and *TMOD1* knockdown in CD34+ erythroid cultures

Tmod1 knockdown studies were carried out using 2 different lentivirally encoded shRNA constructs against TMOD1 derived from TMOD1 MISSION shRNA Bacterial Glycerol Stock (Clone ID: NM_003275.2-512s21c1, TRCN0000330827 and NM_003275.2-553s21c1, TRCN0000330828; Sigma Aldrich). Lentivirally encoded shRNA to luciferase was used as a control. Following differentiation of cord blood CD34+ cells for 2 days, cells were resuspended in 10% FBS IMDM supplemented with 3U/mL heparin and 8μg/mL polybrene, and lentivirus was added at 15 x 10^6 viral particles per 250,000 cells. Cultures were spinoculated via centrifugation for 2 hours at RT and 3000rpm. After overnight incubation at 37^{o}C, transduced cells were placed back in phase I media. After 24 hours, positively transduced cells were selected for by the addition of 1μg/mL puromycin. Puromycin administration was maintained until Day 7 of culture, and erythroid differentiation and enucleation assays were performed as described above.

qRT-PCR

RNA isolations were performed following manufacturer's instructions (RNeasy Plus, Qiagen). cDNA was generated from 1μg of RNA using SuperScript VILO Master Mix (Life technologies),

and gene expression assessed by quantitative PCR using a QuantiStudio 3 Real-Time PCR system (Life Technologies). Gene expression levels were analyzed in triplicate and target mRNA levels were normalized to *ACTB* expression. Relative changes in gene expression were determined by the following equation: $\text{Efficiency}^{\Delta Ct\ \text{reference}}/\text{Efficiency}^{\Delta Ct\ \text{target}}$.

Western Blot

Cells were lysed in 1X Laemmli sample buffer (BioRad) under reducing conditions. Viscosity was reduced by addition of 25U of Benzonase® Nuclease (Millipore) and samples were boiled for 5 minutes. 2 X 10^5 cell lysate equivalents were separated by SDS-PAGE and further steps were performed as described[5].

References

1. Kusakabe M, Hasegawa K, Hamada M, et al. c-Maf plays a crucial role for the definitive erythropoiesis that accompanies erythroblastic island formation in the fetal liver. *Blood*. 2011;118(5):1374-1385.
2. Liu J, Zhang J, Ginzburg Y, et al. Quantitative analysis of murine terminal erythroid differentiation in vivo: novel method to study normal and disordered erythropoiesis. *Blood*. 2013;121(8):e43-49.
3. Hu J, Liu J, Xue F, et al. Isolation and functional characterization of human erythroblasts at distinct stages: implications for understanding of normal and disordered erythropoiesis in vivo. *Blood*. 2013;121(16):3246-3253.
4. Yoshida H, Kawane K, Koike M, Mori Y, Uchiyama Y, Nagata S. Phosphatidylserine-dependent engulfment by macrophages of nuclei from erythroid precursor cells. *Nature*. 2005;437(7059):754-758.
5. Gokhin DS, Lewis RA, McKeown CR, et al. Tropomodulin isoforms regulate thin filament pointed-end capping and skeletal muscle physiology. *J Cell Biol*. 2010;189(1):95-109.

Supplemental Figure Legends, Tables and Movies:

Supplemental Figure 1. Mouse fetal liver erythroblast morphology and F-actin organization during enucleation visualized by confocal microscopy of cells in wet mounts, and by structured illumination microscopy. (A) Extended-focus projections of confocal Z stacks of mouse fetal liver erythroblasts at various stages of enucleation that were not cytospun. Cells were immunostained for Ter119, phalloidin for F-actin, and Hoechst for nuclei and imaged as described in Methods. Sample was prepared for imaging as a wet mount on a slide, sealing the coverslip using Valap (Vaseline, Lanolin, and Paraffin wax mixed in equal amounts at 70^{o}C). (B) Structured illumination microscopy (SIM) of mouse fetal liver erythroblasts in various stages of enucleation immunostained for Ter119, phalloidin for F-actin, and Hoechst for nuclei and mounted on a slide by cytospinning. Cells were imaged using a 100X objective lens (N.A. 1.42) on a Nikon N-SIM microscope. Bars, 4μm.

Supplemental Figure 2. Mouse bone marrow and spleen erythroblast enucleation are qualitatively similar to mouse fetal liver erythroblast enucleation. (A) Extended-focus projections of confocal Z stacks of mouse bone marrow erythroblasts at various stages of enucleation immunostained for Ter119, phalloidin for F-actin, and Hoechst for nuclei. Arrows show a cytoplasmic F-actin spot following the translocating nucleus as it is expelled from the erythroblast. (B) Extended-focus projections of confocal Z stacks of erythroblasts harvested from phlebotomized mouse spleen at various stages of enucleation immunostained for Ter119, phalloidin for F-actin, and Hoechst for nuclei. Arrows show cytoplasmic F-actin spot following the translocating nucleus as it is expelled from the erythroblast. Bars, 4 μm.

Supplemental Figure 3. Mouse fetal liver erythroblast nuclei assume a dumbbell-shaped morphology during enucleation *in vivo*. (A) H&E-stained paraffin sections of E14.5 mouse fetal livers. Black arrows, non-polarized erythroblasts. White arrowheads, dumbbell-shaped nuclei associated with enucleating erythroblasts. Bar, 10 μm. (B) Transmission electron micrographs of mouse fetal liver erythroblasts at various stages of enucleation. R, reticulocyte; P, pyrenocyte. Bars, 2 μm.

Supplemental Figure 4. Mouse bone marrow erythroblasts do not exhibit a continuous F-actin ring during enucleation as is observed in dividing cells during cytokinesis. (A) 3D reconstructions of confocal Z-stacks of (a-c) mouse bone marrow erythroblasts at various stages of enucleation immunostained for Ter119, phalloidin for F-actin, and Hoechst for nuclei. Also shown is F-actin in regions at the Ter119-sorting boundary, defined by yellow brackets, of (a'-c') mouse bone marrow erythroblasts rotated 90° around the axis running perpendicular to the direction of nuclear expulsion, providing a view through the neck of the enucleating erythroblast. In mouse bone marrow erythroblasts F-actin exhibited small gaps (b') and/or large F-actin-free regions (a' and c'). Dashed yellow lines demarcate the location of the nuclear perimeter in the neck region. 3D grid dimensions are indicated. (B) 3D reconstructions of confocal Z-stacks of dividing mouse FL cells undergoing cytokinesis stained with phalloidin for F-actin and Hoechst for DNA. Also shown are regions, defined by yellow brackets rotated 90° around the axis running perpendicular to the direction of cell division, showing a continuous F-actin ring around the cleavage furrow.

Supplemental Figure 5. mDia2 and Arp3 do not colocalize with the F-actin spot at the rear of the translocating nucleus or with the F-actin foci at the neck during mouse fetal liver erythroblast enucleation. (A) Confocal images of mouse FL

erythroblasts at various stages of enucleation (rows 1-5) or cell division (bottom row) immunostained for mDia2 and Ter119, phalloidin for F-actin, and Hoechst for nuclei. Merges, mDia2 (green) and F-actin (red). (B) Confocal images of mouse FL erythroblasts at various stages of enucleation immunostained for Arp3 and Ter119, phalloidin for F-actin, and Hoechst for nuclei. Merges, Arp3 (green) and F-actin (red). Arrows, bright F-actin spots in the cytoplasm of polarized or enucleating cells. Neither mDia2 nor Arp3 is detected in the F-actin spots in polarized or enucleating erythroblasts at any stage of enucleation. Arrowheads, enrichment of mDia2 at the cleavage furrow of a dividing erythroblast. Asterisk, a nonerythroid cell (Ter119-negative) stains very brightly for mDia2 in contrast to relatively dim mDia2 staining in polarized or enucleating erythroblasts. Images are confocal single optical sections, except for fourth and fifth rows of mDia2-stained cells, which are extended focus projections of confocal Z stacks, acquired as in Methods. Bars, 4 μm.

Supplemental Figure 6. Tmod3 does not colocalize with the F-actin foci in polarized or enucleating mouse fetal liver erythroblasts, and Tmod3 levels in fetal liver erythroblasts are not increased in the absence of Tmod1. (A) Extended focus projections of confocal Z stacks of wild-type (top) and *Tmod1*$^{-/-}$ (bottom) mouse FL cells immunostained for Ter119 and Tmod3, phalloidin for F-actin, and Hoechst for nuclei. Merges show Ter119 (green), Tmod3 (red), and Hoechst (blue). Tmod3 staining intensity appears similar in Ter119-positive erythroblasts in wild-type and *Tmod1*$^{-/-}$ fetal liver cells. Asterisks, enucleating erythroblasts. Bar, 8 μm. (B) Confocal single optical sections of wild-type and *Tmod1*$^{-/-}$ mouse FL erythroblasts at various stages of enucleation, immunostained for Ter119 and Tmod3, phalloidin for F-actin, and Hoechst for nuclei. Arrows, cytoplasmic F-actin spots in polarized or enucleating cells. Tmod3 staining is diffuse in the cytoplasm and does not appear enriched in the cytoplasmic F-

actin spot(s) in either wild-type or *Tmod1*$^{-/-}$ FL erythroblasts. Bars, 4 μm. Confocal images were collected using a Zeiss 100X objective lens at zoom 1 (A) or zoom 2 (B).

Supplemental Figure 7. Human bone marrow erythroblast enucleation is characterized by spherical nuclear morphology. Brightfield micrographs of May-Grunewald-Giemsa-stained smears (top) and H&E-stained trephines (bottom) of human bone marrow specimens from patients with the indicated pathological conditions. Top-right panels show erythroblasts at various stages of enucleation. HS, hereditary spherocytosis. DBA, Diamond Blackfan anemia. Bars, 5 μm.

Supplemental Figure 8. Sorting strategy for measuring enucleation during *in vitro* cultures. (A) Flow cytometry analysis of GPA levels after days 11 and 15 of culture in either luciferase control or *TMOD1* knockdown CD34+ cells induced towards erythroid differentiation as described by Hu *et al.*[1]. (B) Late erythroblasts were flow sorted based on the expression levels of α4-integrin and Band 3 (box) and these populations, corresponding to late orthochromatic erythroblasts were subjected to an enucleation assay using SYTO60, as described previously[2]. Briefly, SYTO60^{Low} cells were counted as enucleated cells, giving the enucleation rate (box) indicated for each flow cytogram.

Supplemental Table 1. Percentage of cell diameter occupied by the nucleus at the Ter119 (mouse) or GPA (human) sorting boundary during mouse fetal liver and human bone marrow erythroblast enucleation. Cell surface diameter was defined as the distance perpendicular to nuclear extrusion at the Ter119- or GPA-sorting boundary (parameter *C* in Figure 1B and 3B). Nuclear occupancy is the extent of the cell surface diameter occupied by the nucleus (parameter *D* in Figure 1B and 3B), expressed as a

percentage ($D/C \times 100$). Note that both the cell surface diameter and nuclear occupancy are markedly lower in mouse erythroblasts than in human erythroblasts at the Ter119- or GPA-sorting boundary, respectively, but neither parameter changes significantly during the enucleation process in both species. N, numbers of individual erythroblasts measured at Early, Mid or Late stages of nuclear expulsion. Images for quantification of mouse fetal liver erythroblast dimensions were obtained by collecting 133 confocal Z stacks of cells prepared from 23 embryos (12 different litters). Images for quantification of human bone marrow erythroblast dimensions were obtained by collecting 73 confocal Z stacks prepared from 6 separate human bone marrow samples. Note that these are the same sets of images used to derive the quantitative data for Early, Mid and Late enucleating cells in Figures 1E-D and 3E-D in the main text.

Supplemental Table 2. Primary antibodies used for immunofluorescence microscopy and flow cytometry.

Supplemental Table 3. Secondary antibodies used for immunofluorescence microscopy.

Supplemental Movies 1, 2, 3. Representative 3D reconstructions of confocal Z-stacks of enucleating mouse fetal liver erythroblasts. Cells were immunostained for Ter119 (green), phalloidin-stained for F-actin (red), and Hoechst-stained for nuclei (blue).

Supplemental Movies 4, 5. Representative 3D reconstructions of confocal Z-stacks of enucleating human bone marrow erythroblasts. Cells were immunostained for GPA (green), phalloidin-stained for F-actin (red), and Hoechst-stained for nuclei (blue).

References:

1. Hu J, Liu J, Xue F, et al. Isolation and functional characterization of human erythroblasts at distinct stages: implications for understanding of normal and disordered erythropoiesis in vivo. *Blood*. 2013;121(16):3246-3253.
2. Yoshida H, Kawane K, Koike M, Mori Y, Uchiyama Y, Nagata S. Phosphatidylserine-dependent engulfment by macrophages of nuclei from erythroid precursor cells. *Nature*. 2005;437(7059):754-758.

Supplemental Figure 1

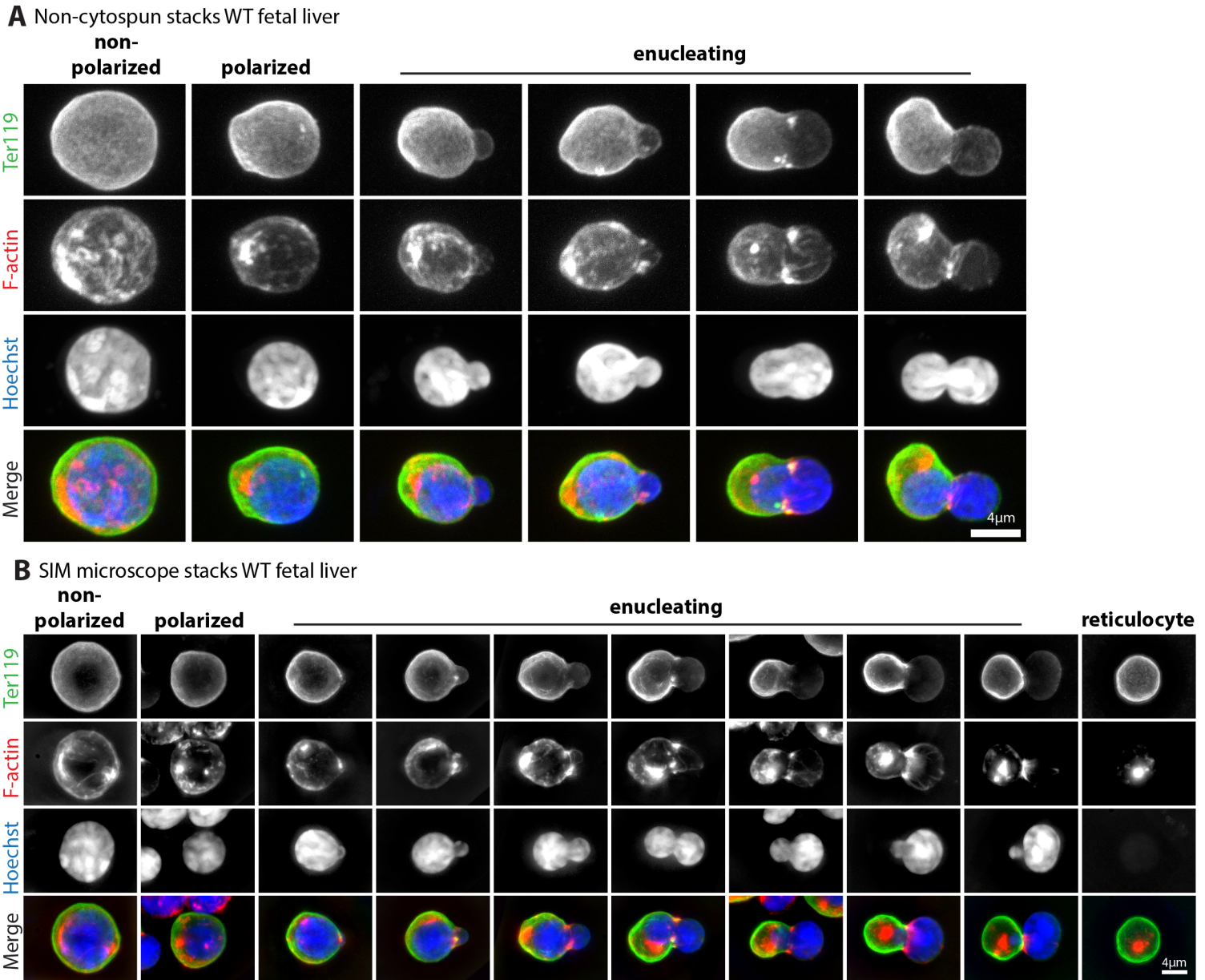

Supplemental Figure 2

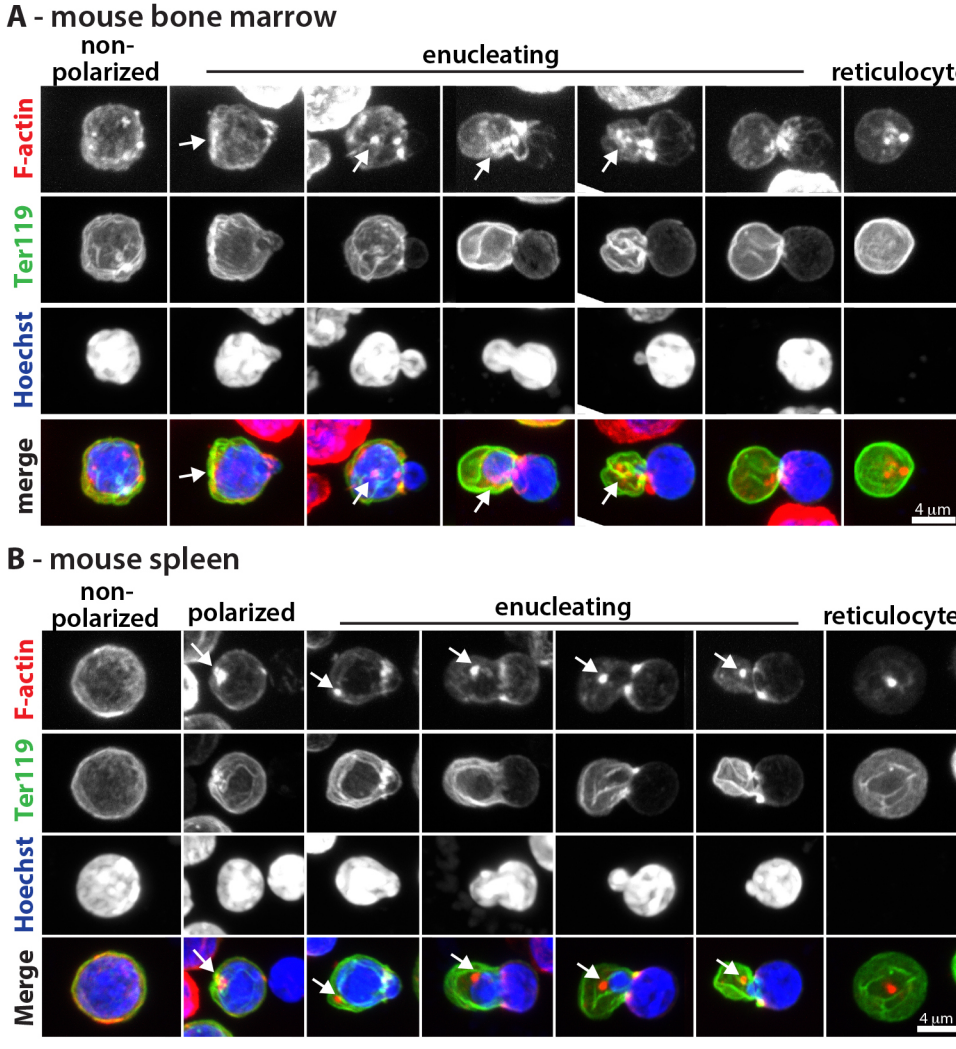

Supplemental Figure 3

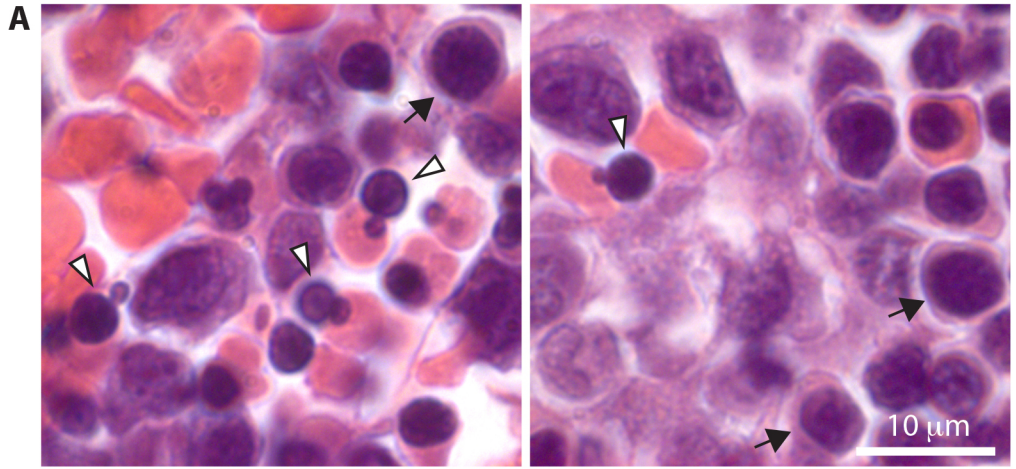

Supplemental Figure 4

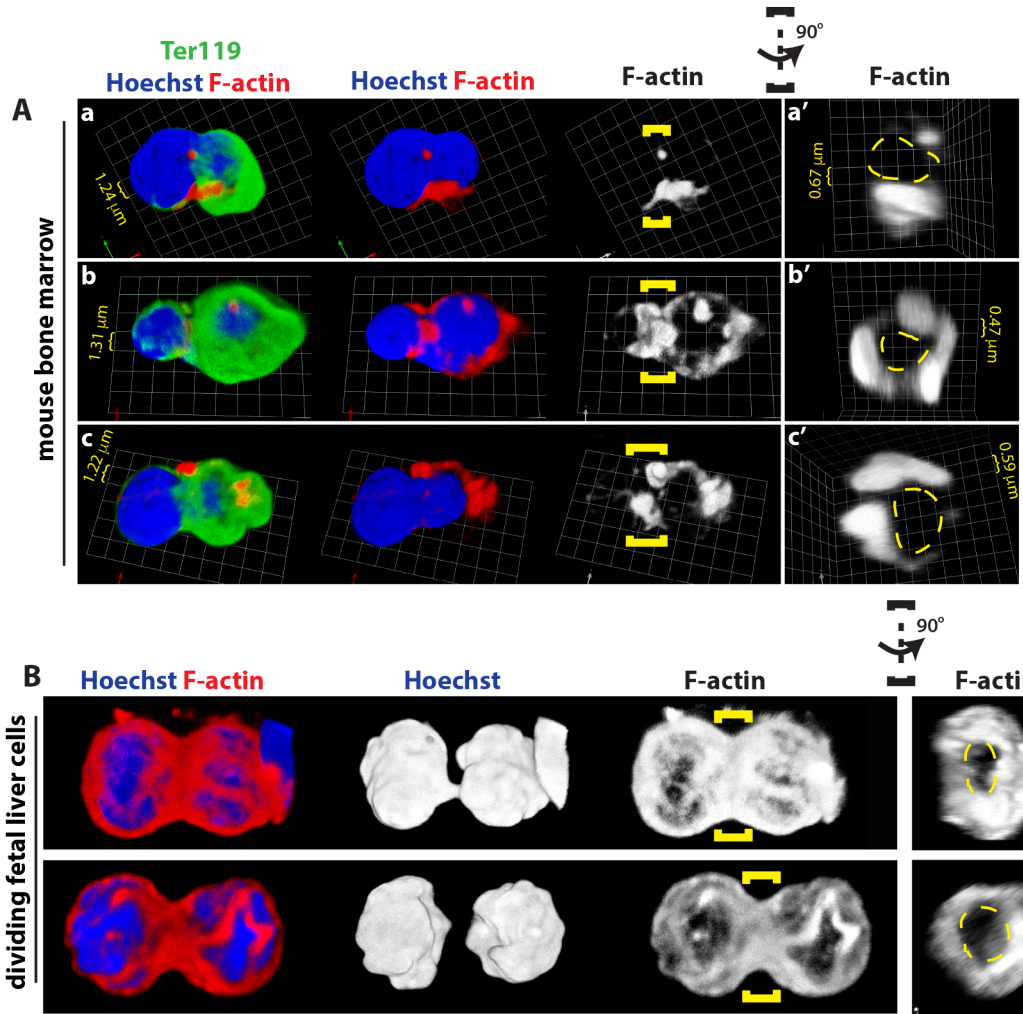

Supplemental Figure 5

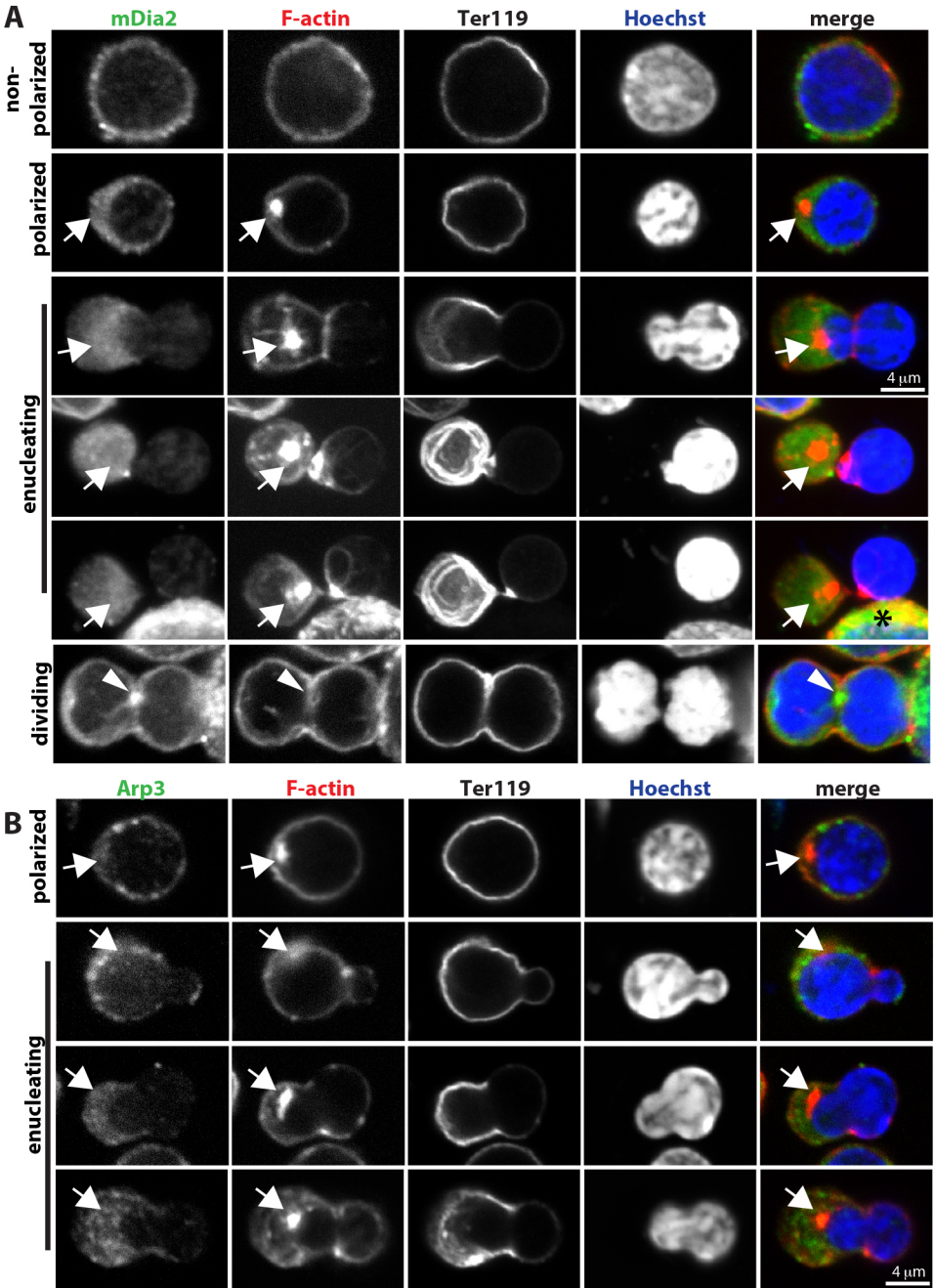

Supplemental Figure 6

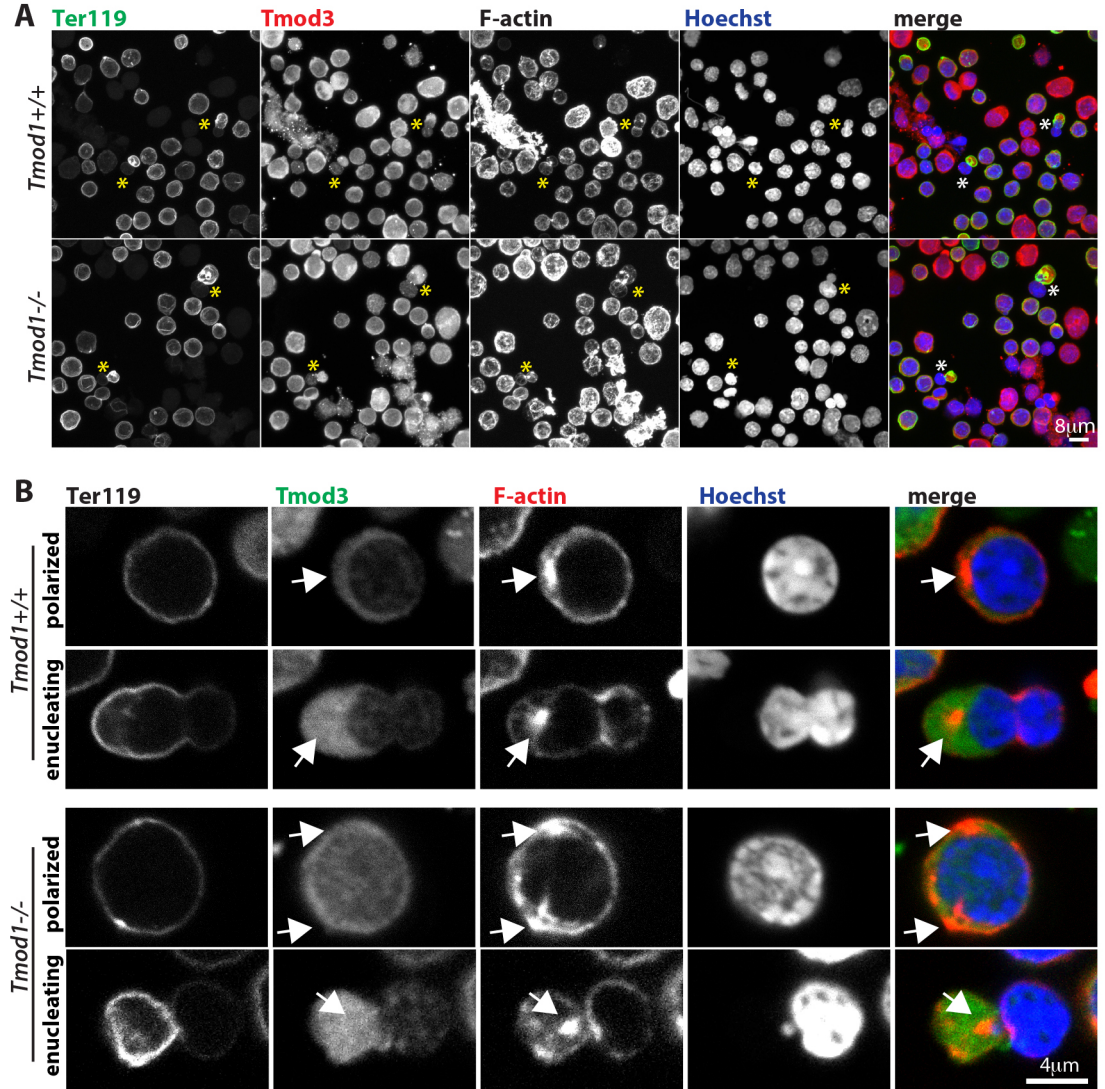

Suplemental Figure 7

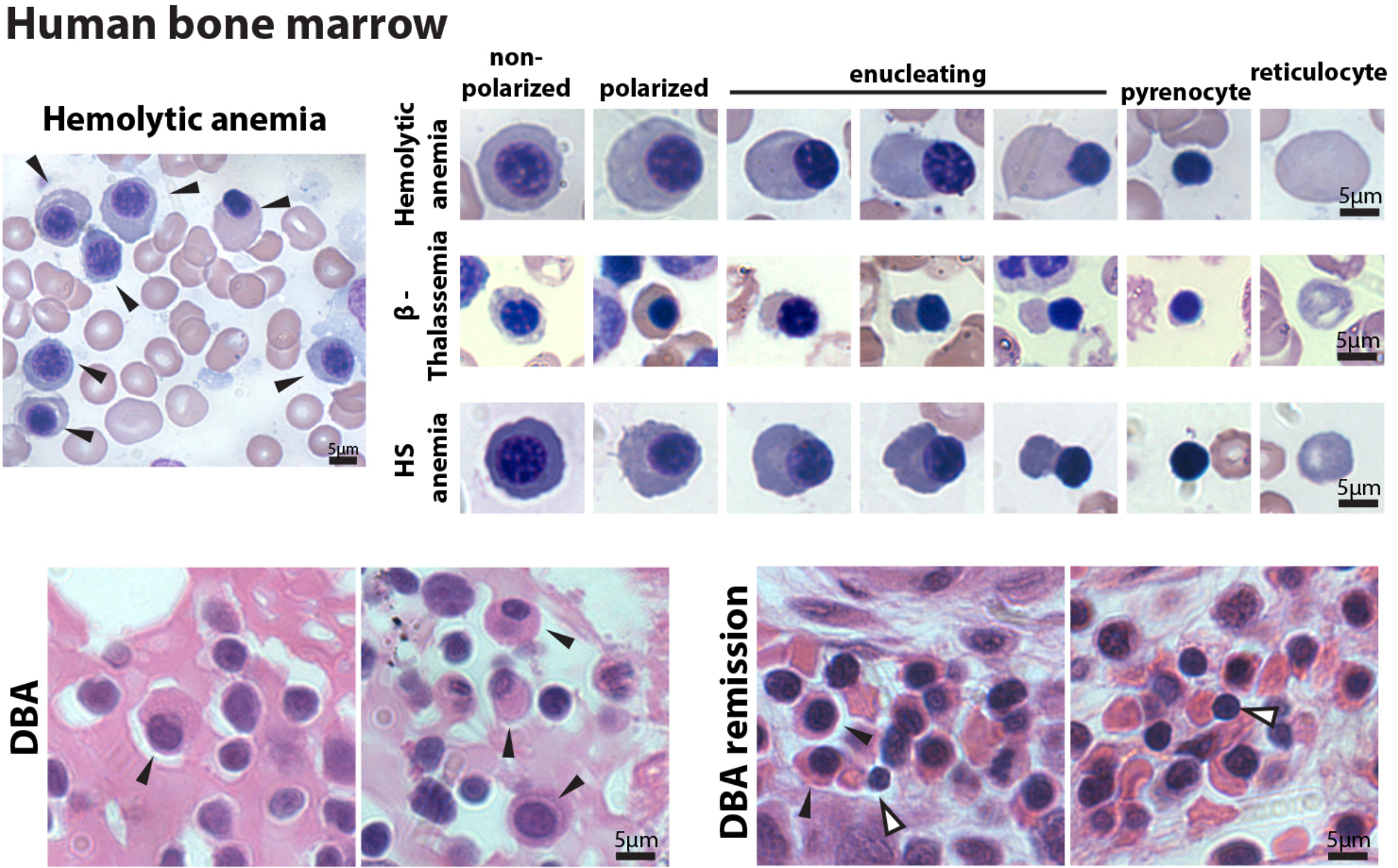

Supplemental figure 8

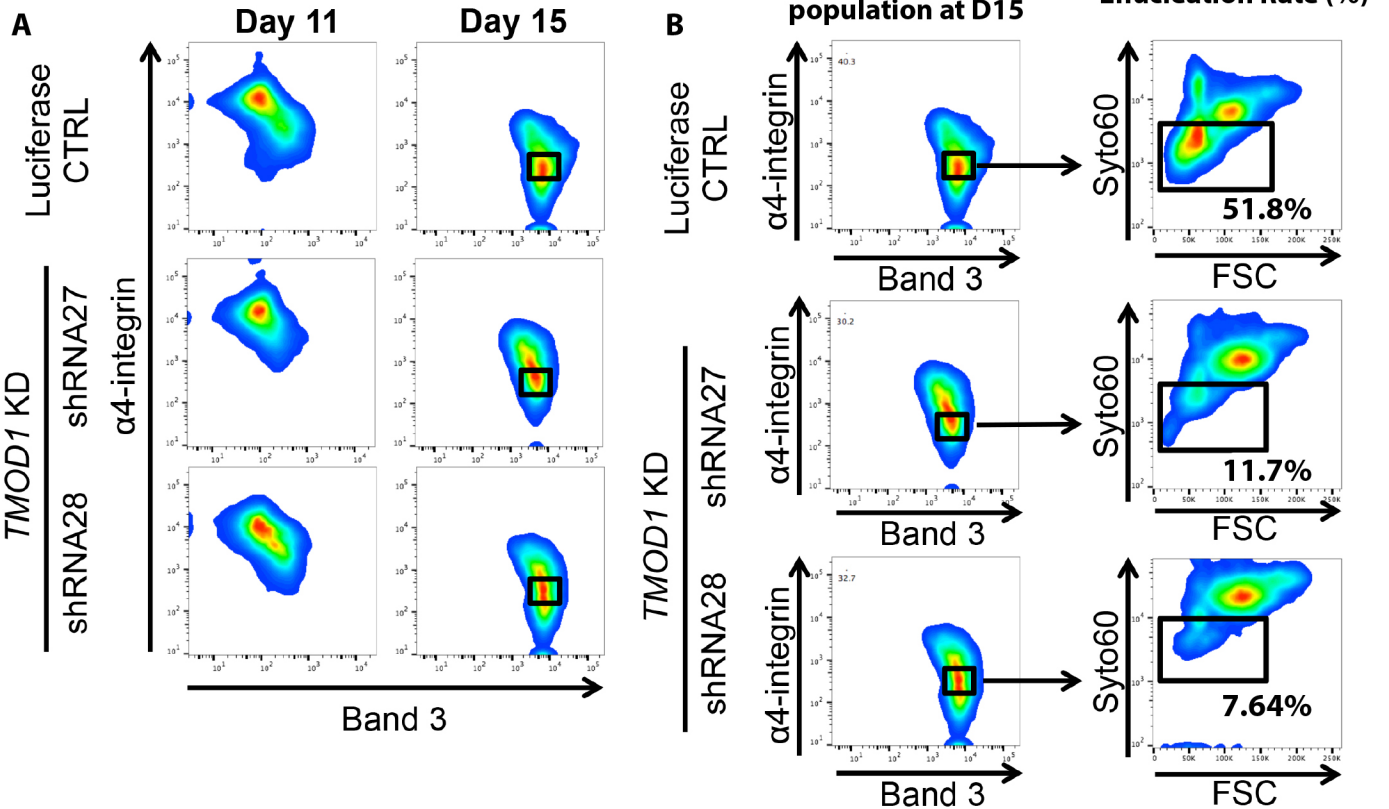

Mouse	n (# of cells)	Cell surface constriction diameter(μm)	Nuclear occupancy (%)
Early	20	2.28±0.70	75.57±14.45
Mid	60	3.14±0.62	76.28±13.71
Late	22	2.64±0.96	71.43±14.35
Human			
Early	8	4.75±1.41	92.61±3.36
Mid	12	5.62±0.81	94.68±9.44
Late	4	5.31±0.67	97.03±2.87

Suppemental Table 1. Percentage of cell diameter occupied by the nucleus at the Ter119 (mouse) or GPA (human) sorting boundary during mouse fetal liver and human bone marrow erythroblast enucleation. Cell surface diameter was defined as the distance perpendicular to nuclear extrusion at the Ter119- or GPA-sorting boundary (parameter C in Figure 1B and 3B). Nuclear occupancy is the extent of the cell surface diameter occupied by the nucleus (parameter D in Figure 1B and 3B), expressed as a percentage (D/C × 100). Note that both the cell surface diameter and nuclear occupancy are markedly lower in mouse erythroblasts than in human erythroblasts at the Ter119- or GPA-sorting boundary, respectively, but neither parameter changes significantly during the enucleation process in both species. N, numbers of individual erythroblasts measured at Early, Mid or Late stages of nuclear expulsion. Images for quantification of mouse fetal liver erythroblast dimensions were obtained by collecting 133 confocal Z stacks of cells prepared from 23 embryos (12 different litters). Images for quantification of human bone marrow erythroblast dimensions were obtained by collecting 73 confocal Z stacks prepared from 6 separate human bone marrow samples. Note that these are the same sets of images used to derive the quantitative data for Early, Mid and Late enucleating cells in Figures 1E-D and 3E-D in the main text.

Supplemental Table 2. Primary antibodies used for immunofluorescence and flow cytometry.

	Species	***Antibody***	***Source***	***Dilution***
NMIIB	Rabbit	M7939	Sigma	1:200
Arp3	Mouse	BD-612134	BD Biosciences	1:50
mDia2	Rabbit	R1358	Gift from Arthur Alberts (Van Andel Institute, Grand Rapids, MI)	1:100
Mouse GPA	Rat	Ter119 (preconjugated)	BD Biosciences	1:60
Mouse CD44	Rat	IM7 (preconjugated)	BD Biosciences	1:130
Mouse CD11b	Rat	MI/70 (preconjugated)	BD Biosciences	1:200
Mouse CD45R	Rat	RA3-6B2 (preconjugated)	BD Biosciences	1:200
Mouse Ly6G/Ly6C	Rat	RB6-8C5 (preconjugated)	BD Biosciences	1:200
Human GPA	Mouse	GA-R2 (preconjugated)	BD Biosciences	1:100
Human α-4 integrin	Mouse	MZ18-24A9 (preconjugated)	Miltenyi Biotec	1:15
Human Band 3	Rabbit	Extracellular region (preconjugated)	Gift from Mohandas Narla, (New York Blood Center, New York, NY)	1:100

LaminA/C	Rabbit	N/A	Gift from Larry Gerace	1:500
LaminB	Goat	M-20	Santa Cruz	1:200
Tmod1	Rabbit	R1749	Fowler laboratory	1:75
Tmod3	Rabbit	R5168	Fowler laboratory	1:50

Supplemental Table 3. Secondary antibodies used for immunofluorescence.

	Fluorophore
Anti-mouse	Alexa 546
Anti-mouse	Alexa 647
Anti-rabbit	Alexa 546
Anti-rabbit	Alexa 647

Goat secondary antibodies were purchased from Invitrogen and used at 1:200.